

Edge Plasma Electrostatic Fluctuation and Anomalous Transport Characteristics in the Sino-United Spherical Tokamak (SUNIST)

**W H Wang¹, Y X He¹, Z Gao¹, L Zeng¹, G P Zhang¹, L F Xie¹, X Z Yang²,
C H Feng², L Wang², Q Xiao¹, X Y Li¹**

¹ Department of Engineering Physics, Tsinghua University, Beijing 100084, China

² Beijing National Laboratory for Condensed Matter Physics, Institute of Physics, Chinese Academy of Sciences
Beijing 100080, China

W H Wang E-mail: whwang@mail.tsinghua.edu.cn

Abstract

In this paper, the edge plasma parameters, including electron temperature T_e , density n_e , plasma potential ϕ_p , radial electric field E_r and the corresponding fluctuations in the SUNIST spherical tokamak have been systematically measured with Langmuir probe arrays. Characteristics of the edge electrostatic fluctuations and the turbulence-induced transport are experimentally investigated. Results show that a naturally formed $E_r \times B_\phi$ poloidal velocity shear layer (VSL) exists near the radial location of the limiter. Wavenumber spectrum analyses show that edge fluctuations have a radial propagation character of the drift wave turbulence, with a characteristic radial phase velocity $v_{phr} \sim 0.7$ km s⁻¹ in SOL and $v_{phr} \sim 0.9$ -1.4 km s⁻¹ in plasma edge, suggesting that the edge turbulence may originate from the core and propagate to the edge via intermittent pattern. A radial profile of the toroidal flow velocity Mach number has been observed, whose maximum is just located at the VSL position, which may imply a possible relation between the poloidal shear flow and the toroidal plasma flow in SUNIST.

1. Introduction

Recently, spherical tokamak (ST) configuration [1] has received considerable attention due to encouraging experimental results [2-8]. ST is a tokamak with low aspect ratio ($A \equiv R/a$ of typically less than 2, where R is the major radius and a is the minor radius). Theoretically, ST plasmas have a few attractive features compared to conventional large-aspect-ratio devices: high β_t (where β_t is the ratio of the plasma pressure to the toroidally magnetic pressure, experimentally, $\beta_t \sim 0.4$ [5]), naturally large elongation ($\kappa \equiv b/a \sim 2$, where b is the vertical radius of the poloidal plasma cross-section) which means extreme reduction in ampere-turns and leads to substantial saving in the cost of the magnet system of a device, good confinement and the possibility of the steady-state operation at modest magnetic field. Some of these advantages have been experimentally identified (e.g. H-mode and energy confinement exceeds conventional tokamak scaling [2-4]), and further research is expected.

Plasma fluctuations are pervasive as a very possible cause of the cross-field anomalous transport in magnetically confined plasmas. But the magnetic geometry of the ST may bring edge plasma fluctuations evident differences in the fluctuation-driven transport and turbulence dynamics, compared to that of the conventional aspect ratio tokamak. For example, theoretically, stronger magnetic field shear and higher β value of the ST may result in more effective suppression of the long wavelength turbulence by both $\mathbf{E} \times \mathbf{B}$ flow shear [9, 10], and a larger ratio of the inboard (favorable field line curvature) versus the outboard (unfavorable field line curvature) magnetic field strength of the ST will be beneficial to the stabilization of electrostatic and electromagnetic high- n instabilities [11]. In addition, according to the theory of sheared poloidal flow generation by the Reynolds stress of turbulence [12,13], the mean poloidal flow generated by the ST edge plasma turbulence may produce different H-mode access requirements from that of the conventional tokamak, which can help distinguish between various bifurcation theories. Therefore, it is crucial important to experimentally investigate the edge plasma fluctuation and turbulent transport characteristics in STs. Such researches have carried out in some devices with different diagnostic tools [14-16], but broader and more extensive studies are obviously needed.

In order to obtain information of anomalous transport and set up the database in an ST device, it is very necessary to simultaneously measure the radial structure of the edge plasma parameters such as electron temperature, electron density, electric field, and plasma rotation, as well as the plasma

electrostatic fluctuations. In this paper, we report the concurrent measurements of these parameters in the Sino-United Spherical Tokamak (SUNIST) with Langmuir probe arrays. Results show that there exists a naturally formed poloidal $E_r \times B_\phi$ velocity shear layer near the radial location of the last closed magnetic flux surface (LCFS). The electrostatic fluctuations of SUNIST have similar saturation characteristics as that shown in the conventional aspect ratio tokamaks.

The remaining sections of this paper are organized as follows: in section 2, the SUNIST device and the experimental setup are described, section 3 is contributed to the experimental results and discussion, conclusions are presented in section 4.

2. Experimental set-up and diagnostics

The SUNIST at Tsinghua University of China is an ST with major radius 0.30 m, minor radius (defined by a set of fixed four-block poloidal limiter) 0.23 m and designed elongation 1.6 [17]. The vacuum vessel consists of two close-fitting hemispherical-like shells made of high magnetic conductivity stainless steel. The two halves were isolated electrically with an especially designed viton ring to cut off the toroidal eddy current in the shells. This viton ring is also used to supply the vacuum sealing and isolation among three parts of the two halves of vessel shells and the central column. The structure of the vacuum vessel and relative locations of the toroidal field coils (TF), the poloidal field coils (PF), the ohmic heating solenoid and the auxiliary induction (compensation field) coils are shown as Figure 1. As the first phase of the construct of this programme, the power supply system can provide 8 ms 13 kA current for the ohmic heating field coils, 100 ms 10 kA for TF and 15 ms 2.0 kA for PF. After overnight baking up to 150 °C with heater sheets pasted on the outer surface of the vessel and wall conditioning with titanium gettering and helium glow discharges, SUNIST achieved first ohmically-heated hydrogen plasma at the end of 2002 with 0.15 Tesla of the toroidal field and 50 kA plasma current.

The primary diagnostics employed in this experiment are three sets of radially moveable Langmuir probe arrays located on the outer side of the equatorial plane of the device, shown as figure 1. Figure 2 illustrates the relative positions of the windows where the probe arrays are laid and the closed-up view of the probe structures. The directions of the plasma current and the toroidal magnetic field are clockwise from top-view. A four-tip probe array (array 1) is installed in the window 1. A

three-tip array (array 2) and a Mach probe are mounted in the window 2, which is separated from the window 1 with toroidal 150° . All tips are made of molybdenum wire 3 mm in length and 1 mm in diameter and 3 mm separation between adjacent tips. Array 1 is operated as a triple probe [18] to obtain the time-averaged and fluctuating electron temperature (T_e , \tilde{T}_e), plasma density (n_e , \tilde{n}_e), and plasma potential (ϕ_p , $\tilde{\phi}_p$). In array 1, tip 1 and tip 3 (poloidally separated about $\Delta_\theta = 4.3$ mm) are used to measure the floating potential (ϕ_f , $\tilde{\phi}_f$). A dc bias of 43 ~ 145 V is loaded between tip 2 and tip 4 to measure the ion saturation current (I_{si} , \tilde{I}_{si}) from tip 2 and the potential V_+ from tip 4, respectively. From tip 1 and tip 3, a fluctuating poloidal electric field $\tilde{E}_\theta(t)$ can be deduced, i.e., $\tilde{E}_\theta(t) = (\tilde{\phi}_{f3}(t) - \tilde{\phi}_{f1}(t)) / \Delta_\theta$, whereby the radial turbulence-induced particle and heat fluxes Γ_r and Q_r can be derived respectively as [19, 20]

$$\Gamma_r = \langle \tilde{n}_e \tilde{E}_\theta \rangle / B_\phi = \frac{2}{B_\phi} \int_0^\infty \tilde{n}_e(f) \tilde{\phi}_f(f) k_\theta(f) |\gamma_{n\phi}(f)| \sin[\alpha_{n\phi}(f)] df, \quad (1)$$

$$Q_r = Q_{conv} + Q_{cond} = \frac{3}{2} T_e \Gamma_r + \frac{3n_e}{2B_\phi} \langle \tilde{T}_e \tilde{E}_\theta \rangle = \frac{3}{2} T_e \Gamma_r + \frac{3}{B_\phi} \int_0^\infty \tilde{T}_e(f) \tilde{\phi}_f(f) k_\theta(f) |\gamma_{T\phi}(f)| \sin[\alpha_{T\phi}(f)] df \quad (2)$$

where B_ϕ is the toroidal magnetic field, Q_{conv} and Q_{cond} are the convective and conductive heat items respectively, the $\gamma_{n\phi}(f)$ ($\gamma_{T\phi}(f)$) and $\alpha_{n\phi}(f)$ ($\alpha_{T\phi}(f)$) are the coherence and phase angle spectra between the fluctuation fields \tilde{n}_e and $\tilde{\phi}_f$ (\tilde{T}_e and $\tilde{\phi}_f$), respectively. For two random fluctuation signals $X_1(t)$ and $X_2(t)$, their auto- and cross-power spectral densities are defined as $P_{11}(f)$, $P_{22}(f)$ and $P_{12}(f)$, so their coherence spectrum $|\gamma_{12}(f)|$ is defined as

$$|\gamma_{12}(f)| = \frac{|P_{12}(f)|}{|P_{11}(f)P_{22}(f)|^{1/2}}. \quad (3)$$

$|\gamma_{12}(f)|$ is used to estimate the degree of cross correlation between $X_1(t)$ and $X_2(t)$. Usually, \tilde{n}_e is directly estimated from the measured \tilde{I}_{si} , assuming the electron temperature fluctuation \tilde{T}_e can be reasonably neglected. In array 2, all three tips (tip 5 is separated radially by 3 mm from other two tips) are used to measure the floating potentials to provide simultaneous measure of the radial wavenumber

and the poloidal wavenumber of the fluctuations, by which the radial and poloidal wavenumber spectra can be calculated [21]. All probe tips are orientated off the magnetic field lines to avoid shadowing of probe tips from each other.

In above measured physical variables, the electron density n_e and plasma potential ϕ_p are determined by the measured I_{si} , ϕ_f and T_e with the Stangeby's model [22]: $n_e = \alpha I_{si} T_e^{-1/2}$, $\phi_p = \phi_f + \mu T_e$, where α is a constant coefficient depended on the geometry size of tips and μ is the sheath potential drop coefficient (taken as 3 in the our experiments).

The Mach probe (see fig. 2) is used to measure the toroidal flow velocity of edge plasma. [23] The Mach probe is an extension of the Langmuir probe. In the case of a plasma with net toroidal flow, the two tips, placed back to back and separated with a mechanical obstruction, will collect different fluxes of particles (proportional to the ion saturation current) in the upstream and downstream directions of the toroidal magnetic field. Under the one-dimensional collisionless kinetic model, considering the viscosity of plasmas, Chung and Hutchinson [23] obtained a relationship between the ratio of the upstream to downstream currents, R_M , and the toroidal drift velocity of the plasma by the form

$$R_M = \exp(Ku_d), \quad (4a)$$

where $K \sim 1.7$ for $T_i \approx T_e$ and u_d is the drift velocity in unit of $\sqrt{T_e/m_i}$. Generally, the relation $T_i \approx T_e$ is roughly satisfied for the edge plasma. If we denotes the Mach number M as $M = v_\phi / c_s$, here the v_ϕ is the plasma toroidal flow velocity and the c_s is the ion sound speed, $c_s = \sqrt{(T_i + T_e)/m_i} \approx \sqrt{2T_e/m_i}$, then the Eq.(4a) can be rewrite as the logarithmic form

$$M \approx 0.35 \ln(R_M). \quad (4b)$$

In our experiment the tip 8 and tip 9 were biased -145 V to measure the upstream and downstream ion saturation current respectively, whereby the ratio R_M can be obtained. Then the M and the toroidal plasma flow velocity v_ϕ can be estimated.

The experiments are carried out in ohmically-heated hydrogen plasma discharges with the toroidal magnetic field $B_\phi = 0.13$ T, the plasma current $I_p = 30$ kA and a loop voltage of 5 V. Normally the plasma discharge durations are 5 ~ 6 ms with a flat-top phase of 2 ms (which is limited by the voltage-second of the ohmic heating solenoid). Such short time discharges and low temperature in edge plasmas allow the probes to be inserted into radially deeper edge plasma region (the part inside

LCFS belonging to the confinement region) without obviously excessive thermal load onto them. A variety of radial profiles are obtained by shot-to-shot measurements. In experiments, the probe arrays in two windows are synchronously moved the same radial interval 5 mm. At each radial position 10 ~ 15 shots identical discharges are conducted to compute statistic averages. All the data for analyses in the paper are taken in the flat-top phase of the plasma current and digitized at 2 MHz with 12-bit resolution using a multichannel digitizer.

Figure 3 shows typical time evolutions of diagnostic signals (shot-number 04010704). Figure 3(a) and 3(b) are the plasma current and loop voltage waveforms respectively. We can see that the discharge ends without the distinct internal reconnection events (IRE) during the current ramp-down phase. Such shots occur in most cases in our experiment. In some shots the IRE are observed in the decay phase of the plasma current, but they have not led to the major disruptions usually caused by the vertical displacement events. The 5 V loop voltage, larger than that in the conventional tokamaks, exhibits the enhancement feature of resistivity of STs due to neo-classical effects. Figure 3(c) and 3(d) are the measured ion saturation current and floating potential, respectively. They clearly show the stationary processes of the time series during the flat-top of the plasma current. This statistical character ensures the validity of probe data in absence of information of the displacement and the profile of plasma current at present.

3. Results and discussion

3.1 Radial profiles of the equilibrium parameters

The radial profiles of equilibrium T_e , n_e , ϕ_f and ϕ_p are shown in figure 4(a) and 4(b), respectively. The horizontal coordinate is the major radius and the shadow region stands for the radial location of the limiter. In the figure and hereafter, the error bars denote the statistical errors of the ensemble average. It can be seen from figure 4 (a) that in the scrape-off layer (SOL, $r > r_{\text{limiter}}$) the T_e and n_e are relatively low ($T_e \sim 10$ eV and $n_e \sim 2 \times 10^{18} \text{ m}^{-3}$) and the profiles are relatively flat (the temperature scale length $L_T = [(1/T_e)(-dT_e/dr)]^{-1}$ and the density scale length $L_n = [(1/n_e)(-dn_e/dr)]^{-1}$ are about the order of 10 cm), whereas in the plasma edge region ($r < r_{\text{limiter}}$), the profiles of the T_e and n_e are steeper ($L_T, L_n \sim 2 - 5$ cm). The edge temperature and density are in the range $T_e = 10 - 60$ eV

and $(5 - 8) \times 10^{18} \text{ m}^{-3}$ respectively, similar to the results obtained in other STs [14,16].

The profiles of the floating potential ϕ_f and the calculated plasma potential ϕ_p are shown in figure 4(b). A seventh-polynomial fit of the ϕ_p profile is also displayed in dotted curve here, from which the radial profiles of the radial electric field $E_r = - (d\phi_p/dr)$ and thereby its radial gradient dE_r/dr can be inferred as shown in figure 5. We can see from fig. 4(b) and fig.5 that the ϕ_p and the dE_r/dr profiles are peaked at $r = 54.5 \text{ cm}$, the vicinity of the radial location of the limiter, where E_r changes its direction from inward in the plasma edge to outward in SOL. So a naturally formed poloidal $E_r \times B_\phi$ velocity shear layer (VSL) is formed in the radial range of probably 1 cm. The VSL has been observed on many tokamaks [24-26]. We also notice in experiments that the variance of discharge parameters only affects the magnitudes of both the E_r and the dE_r/dr but does not change the radial location of the maximal shear of the dE_r/dr .

A radial profile of the plasma toroidal flow velocity Mach number, M , calculated with Eq. (4b), is shown in figure 6. In SOL, $M \sim 0.1$ and the estimated toroidal velocity v_ϕ is about 3.4 km s^{-1} , but in the plasma edge they are about four times the former, i.e. $M \sim 0.4$ and $v_\phi \sim 13 \text{ km s}^{-1}$. A maximal radial gradient of the v_ϕ appears at the radial location of the VSL. Such coincidence was the first observed on the TEXT-U tokamak [27], but it seems not to be reported on STs so far. This result may imply a possible relation between the poloidal shear flow and the toroidal plasma flow in STs. [28] We will further research it in next experiment.

3.2 Fluctuations and the turbulence-driven transport characteristics

Figure 7 shows radial profiles of the absolute root-mean-square (RMS) fluctuation magnitude \tilde{n}_e , \tilde{T}_e and $\tilde{\phi}_p$ (a) and their relative fluctuation levels \tilde{n}_e/n_e , \tilde{T}_e/T_e and $e\tilde{\phi}_p/kT_e$ (b). We can see that at all measured radii, both SOL and the plasma edge, there exist $\tilde{n}_e/n_e \sim (2-3)\tilde{T}_e/T_e$. We also notice that for the radial positions $r \geq 52 \text{ cm}$, there exists $\tilde{n}_e/n_e \neq e\tilde{\phi}_p/kT_e$, i.e. the data deviates from the simple Boltzmann relationship in plasma edge region. But at the radial positions $r \leq 52 \text{ cm}$, the \tilde{n}_e/n_e and $e\tilde{\phi}_p/kT_e$ become comparable and have nearly the same size within the experimental errors. In other words, the Boltzmann relationship is roughly obeyed in the $r \leq 52 \text{ cm}$ radial positions.

According to the theoretical predictions of drift wave propagation present by Mattor and Diamond [29-31] that the edge turbulence is come from the adiabatic core region where the Boltzmann relationship, $\tilde{n}_e/n_e \approx e\tilde{\phi}_p/kT_e$, is satisfied. So the region where the $r \leq 52$ cm may be reasonably judged as the region close to the plasma core. This result is also similar to the observations in other tokamaks. [32, 33]

We analyzed the radial propagating characters of fluctuations with the standard two-point cross-correlation technique [21]. This technique provides a highly localized wavenumber-frequency spectral density $S(k, f)$ estimate, especially suited for the investigation of the low-frequency ($f < 500$ kHz) and long-wavelength ($\lambda > 5$ mm) components of the turbulence, requiring samples at only two points in space. The method can be roughly outlined as follows. Firstly, we break the raw data from tow fixed spatial points (radial or poloidal) into many contiguous intervals. For each interval we compute the auto- and cross-power spectra. From the phase of the cross-power spectrum $\alpha_{X_1 X_2}^j(f)$ (where j is the serial number) a local wavenumber $k^j(f) = \alpha_{X_1 X_2}^j(f)/d$ can be estimated (where d is the separation between the two tips of the probe). Then we define the average power associated with a given frequency and local wavenumber to be the local wavenumber spectrum, $S(k, f)$. The local wavenumber spectrum is a good estimate of the conventional spectrum for a stationary time series (in other words, the local wave amplitude and the local wave number vary slowly over a wavelength, a detailed description refers to Ref. [21]). The third step is to calculate the normalized local wavenumber spectral density $s(k, f) = S(k, f) / \sum_{k, f} S(k, f)$ and $s(f) = \sum_k s(k, f)$, from which we can estimate a series of physical quantities characterizing the edge plasma turbulence: the conditional spectral density $s(k_r | f) = s(k, f) / s(f)$; the spectral-averaged statistical dispersion relation $k(f) = \sum_k k \cdot s(k|f)$; the wavenumber spectral width $\sigma_k(f) = \left[\sum_k (k - k(f))^2 \cdot s(k|f) \right]^{1/2}$; the spectral-averaged wavenumber $\bar{k} = \sum_f k(f) s(f)$ and the turbulence propagating phase velocity $V_{ph} = \sum_{k, f} \frac{2\pi f}{k} s(k, f)$, etc.

Figure 8 shows some spectral-analyzed results of the floating potential fluctuations. A typical contour plot of the conditional wavenumber-frequency spectrum $s(k_r | f)$ at $r = 50$ cm is shown in figure 8(a). The corresponding radial wavenumber spectrum $S(k_r)$, the spectral-averaged statistical dispersion relation $k_r(f)$ and the wavenumber spectral width $\sigma_{k_r}(f)$ are present in figure 8(b) and 8(c),

respectively. In figures, the positive wavenumber corresponds to the propagation in radially outward direction. The fluctuation power is primarily confined to frequencies $f \leq 200$ kHz and wavenumbers $0 \leq k_r \leq 4 \text{ cm}^{-1}$. The spectra have both positive and negative k_r components but the positive case is greater. Such asymmetries of $s(k_r|f)$ can be further quantified by the dispersive properties, which means a net radial outward propagation of the electrostatic fluctuations. Figure 8(c) displays a linear-like feature of the $k_r(f)$ versus f that implies a same radial propagation velocity over the frequency band 0-200 kHz. Moreover, in this frequency band the wavenumber spectral width has a broadband feature of $\sigma_{k_r}(f) \geq k_r(f)$. All of these features indicate that the edge fluctuations on SUNIST are the fully developed turbulence and have a quasi-mode structure of the radial drift wave modes [31].

We observed the statistical characteristics at all measured radii and similar results are obtained. The radial profiles of the radial spectral-averaged wavenumbers \bar{k}_r and the radially propagating phase velocity v_{phr} are shown in figure 8(d). It is clear to see that at all radial locations the $\bar{k}_r > 0$, and the \bar{k}_r changes little ($\bar{k}_r < 1 \text{ cm}^{-1}$) with radial locations in plasma edge region but increases ($\bar{k}_r > 1 \text{ cm}^{-1}$) with the probes moving radially outwards in SOL. In contrast, the v_{phr} remains approximately constant ($v_{phr} \sim 0.7 \text{ km s}^{-1}$) in SOL but raises with inward radial locations ($v_{phr} \sim 0.9\text{-}1.4 \text{ km s}^{-1}$). The radial velocity of the turbulence resembles the results of the radial moving velocity of the ‘blob’ structures measured by the gas puff imaging technique in NSTX [14], so it may be a signature of the self-organized structures motion in SUNIST edge. These results support the predictions of the radial drift wave propagation theory proposed by Mattor and Diamond [31-33] that edge turbulence may originate from core fluctuations propagating to the edge. Similar results have been observed in diversified magnetic confinement devices with different diagnostic tools [14, 34-39], which reveal the common nature of the edge fluctuations almost invariable to the size, configuration and discharge parameters of devices.

Applying the local k - f spectrum method to the poloidal fluctuation data we obtained the poloidal features of the turbulence. Figure 9(a) displays the radial profile of the poloidal spectral-averaged wavenumber \bar{k}_θ . The positive direction denotes the electron diamagnetic direction. We can see that the \bar{k}_θ is in the range of 0-1 cm^{-1} , and at VSL location the \bar{k}_θ changes its poloidal propagation

direction from the electron diamagnetic direction in the plasma edge region to the ion diamagnetic direction in SOL. Figure 9(b) presents a comparison of radial profiles of the poloidal and radial correlation lengths $l_{c\theta}$ and l_{cr} . Here the correlation length is defined as the inverse of the spectral-averaged wavenumber spectral width $l_c \equiv \bar{\sigma}_k^{-1}$. It shows that the poloidal correlation length $l_{c\theta} \approx 2\text{-}2.5$ cm and the radial correlation length $l_{cr} \approx 1.5$ cm. Both remain roughly constant with a little increase in SOL. So there exists $l_{c\theta}/l_{cr} \approx 1.3\text{-}1.6$ in SUNIST edge. These results are different from the results measured in the conventional aspect tokamaks [35, 36] and stellarators [37] where the $l_{c\theta}$ is about 1 cm and over twice longer than the l_{cr} . A longer poloidal correlation length that $l_{c\theta} \approx 4$ cm (and $l_{cr} \approx 3$ cm but was defined differently) has also been obtained in NSTX with the gas puff imaging diagnostic method [14]. A possible explanation, as Zweben mentioned [14], is the magnetic geometry of STs, which has a much larger ratio of poloidal field to toroidal field at the outer midplane.

We calculated the turbulence-induced particle and heat transport fluxes Γ_r and Q_r with equations (1) and (2). The radial profiles of the Γ_r and Q_r are shown in figure 10(a) and 10(b). Both fluxes decrease towards the edge. In figure 10(a) a small dip in the Γ_r profile can be found at the VSL location, which is beyond the interpretation of errors. According to Eq. (1), not only the absolute fluctuation magnitudes \tilde{n}_e and $\tilde{\phi}_f$ ($\sim \tilde{\phi}_p$) contribute to the Γ_r , but the spectral-averaged coherence $\bar{\gamma}_{n\phi}$ and the phase angle $\bar{\alpha}_{n\phi}$ may also be important for the Γ_r . To prove this, we calculated $\bar{\gamma}_{n\phi}$ (and $\bar{\gamma}_{T\phi}$) and $\bar{\alpha}_{n\phi}$ (and $\bar{\alpha}_{T\phi}$) in all measured radii as shown in figure 10(c) and 10(d). It is obvious that in the vicinity of the VSL location, $\bar{\gamma}_{n\phi}$ (and $\bar{\gamma}_{T\phi}$) reaches its minimum of the radial profile, and $\bar{\alpha}_{n\phi}$ (and $\bar{\alpha}_{T\phi}$) changes its direction, both of which tend to make Γ_r smaller. In figure 10(b), the convective and conductive items Q_{conv} and Q_{cond} are present. It is clear that the Q_r is mainly contributed by the convective transport item Q_{conv} simply because of the $\bar{\gamma}_{n\phi} > \bar{\gamma}_{T\phi}$ (fig. 10(c)) and $\tilde{n}_e/n_e > \tilde{T}_e/T_e$ as well (fig. 7(b)).

Intermittency or the large transport events is an important feature of the cross-field particle transport in magnetic confinement devices. This intermittent transport has both quasi-coherent structures in small (temporal and spatial) scale and long-range correlation (in global, or system scale) properties in statistics. In this paper, we refer to the events with short time scale as the intermittent

events to distinguish themselves from the long-range correlation events, or “bursty” events. There have been extensively documented works about intermittent transport in tokamaks [40-43], stellarators [44] and RFP [45]. Here we report our observations in SUNIST edge and preliminary results of them. Figure 11(a) and 11(b) are the time evolution episodes (1 ms) of the local particle fluxes from two different radial locations $r = 52$ cm (in plasma edge) and $r = 57$ cm (in SOL). Here the time-resolved particle flux $\Gamma_r(t)$ is calculated directly by multiplying $\tilde{n}_e(t)$ and $\tilde{E}_\theta(t)$ together $\Gamma_r(t) = \tilde{n}_e(t) \times \tilde{E}_\theta(t)$. We can see that the fluctuations of $\Gamma_r(t)$ have different patterns. In SOL, the $\Gamma_r(t)$ performs as a Gaussian-like noise with short-time scale intermittency, but in plasma edge, the $\Gamma_r(t)$ looks more like “bursty”. Such time patterns of fluctuations and fluxes are universal in our experiments, not only for the particle and heat transport fluxes, but also for the ion saturation current \tilde{I}_{si} , floating potential $\tilde{\phi}_f$. On account of the length of this paper, hereafter we only focus on the $\Gamma_r(t)$ analysis. A convenient quantitative analysis tool for intermittent events is the conditional averaging technique [46], which allows us to characterize a coherent structure in a signal. We take $3 \times \tilde{\Gamma}_r / \Gamma_r$ as threshold value, i.e. those events ($\pm \tau = 50 \mu\text{s}$) whose relative amplitudes are above $3 \times \tilde{\Gamma}_r / \Gamma_r$ are picked out of the initial time series with a given window to reconstruct a new subsequent averaged series. Figure 11(c) and 11(d) are results corresponding to data in figure 11(a) and 11(b), where N denotes the number of the intermittent events occurring in the whole 2 ms time series for each signal. We can see that all events, both from the SOL and the plasma edge, have an about $30 \mu\text{s}$ characteristic time width, the typical fluctuation time scaling. In the plasma edge ($r = 52$ cm), the number of the events occurs fewer than that from the SOL ($r = 57$ cm), but the amplitude of events are higher (double times than the latter), similar to the result of the DIII-D.[47]

Statistically, the intermittent transports always behave the long-range correlation characteristics like avalanches do. The probability distribution functions (PDFs) and auto-power spectrum technique often be used to describe the dynamics of these large transport events. In this paper we use them to our particle flux data and show results as figure 12. Here we applied the method suggested by Carreras [48] to calculate the PDF of fluxes. Firstly, we normalized the fluxes to their averaged values, $\Gamma_n \equiv I(t) / \langle I(t) \rangle$. Then we calculated the flux PDF according to following method:

$$p(\Gamma_n) = N_\Gamma / N, \quad (5)$$

where N_r is the number of values of Γ_n that fall within the range $\Gamma_n \pm W/2$, W is the interval length centered at Γ_n and N is the total number of data points in $\Gamma(t)$. Typically, the value of Γ_n is in the range -20 to 20 , and the full range of Γ_n is divided into 80 intervals of equal length ($W = 0.5$). Finally, we do a similarity transformation $p(\Gamma_n) \rightarrow p(\Gamma_n) \times \langle \Gamma(t) \rangle$ to have a comparable function form for all measured positions. Figure 12 (a) is the *PDFs* of the $\Gamma_r(t)$ from two radial locations (data is the same as in figure 11(a)). We can see that both *PDFs* have a clear positive non-Gaussian long-time lag tails, which are the signature of long-range correlation transport events. Furthermore, the *PDF* from the plasma edge has a little larger tail than that from SOL. Integrating the positive tail of the *PDF* can give information of the contribution of the outward large transport events to the overall outward flux. The results indicate that, for the plasma edge case, such contribution, happening within $\sim 7\%$ of the time, may account for 50% of the total particle transport. Contrastively, in SOL case the largest 10% of the flux events is needed to carry the same fraction of the total flux. It means that more importance of the large but infrequent transport events for the edge than that for the SOL.

Two auto-power spectra of the Γ_r at the same locations as in figure 11(a) are shown in figure 12(b). Each spectrum results from averaging over 10 \sim 15 samples from reproducible discharges with 4096 points (2 ms) for each sample. It is obvious that both spectra can be divided into two frequency ranges: a low frequency end of spectrum which extend about two frequency decades and ended at frequency $f \sim 70$ kHz, called mesoscale frequency range. This range is dominated by the larger-scale transport events and is usually called the long-time correlation range. The other frequency range occurs at high-frequency end of spectrum, $f > 70$ kHz, and is dominated by short-time-scale transport events. In mesoscale frequency range, the spectra display an approximately $f^{-\zeta}$ power law behavior with an spectral exponent $\zeta_1 < 1$. The ζ_1 is an indication of the long-range correlation character of a time series with stationary processes. Larger value of the ζ_1 means more long-range correlation transport events. Whereas for high-frequency range of the spectra, a larger exponent $\zeta_2 (> 1)$ stands for less number of the small-scale transport events. The spectral exponent ζ can be calculated with the octave binning method proposed by Anthony Davis [49]. To make a clear comparison of the spectra between the edge case and the SOL case in one chart, the values of the spectrum for the radial location $r = 52$ cm are multiplied by factor 10. It can be seen that for the plasma edge case the $\zeta_1 = 0.63$, larger than the value of the SOL case ($\zeta_1 = 0.58$), indicating more of the long-range correlation transport

events in plasma edge. Correspondingly, at high-frequency range the spectral exponent of the edge case ($\zeta_2 = 3.34$) is also larger than that in SOL ($\zeta_2 = 2.87$), implying that the number of the small-scale transport events is less in the edge than in the SOL. These results are consistent with results of the PDF analysis (Fig. 12(a)) and the conditional averaging (Fig. 11(c) and (d)).

According to the hypothesis of the dynamical origin of the fluctuation structures described by Carreras B A *et al.* [50], the intermittent transport events, as non-diffusive fluctuation structures, could be coming from the plasma core, be decorrelated and broken when they cross the edge shear flow layer, and reform again in the SOL. Results from our experiments, especially the one from plasma edge support this assertion. Of course, to further confirm this point needs a deeper analysis, which cover near-core measurement and several diagnostics application to corroborate each other, etc. Such experiment is under way in SUNIST tokamak.

4. Conclusions

In this paper, we made systematic measurements for edge plasma parameters, electron temperature T_e , electron density n_e , plasma potential ϕ_p , radial electric field E_r and their corresponding fluctuations in SUNIST spherical tokamak with high poloidal, radial (both 3 mm) and temporal (0.5 μ s) resolution Langmuir probe arrays. The characteristics of the edge electrostatic fluctuations and the turbulence-induced transport are experimentally investigated. Results show that there exists a naturally formed electric field near the radial location of the limiter, whereby a $E_r \times B_\phi$ poloidal velocity shear layer is formed. Radial wavenumber spectrum analyses show that edge fluctuations have radial propagation character of the drift wave turbulence, with a characteristic radial phase velocity $v_{phr} \sim 0.7$ km s⁻¹ (in SOL) and $v_{phr} \sim 0.9-1.4$ km s⁻¹ (in plasma edge), suggesting that the edge turbulence may originate from the core via intermittent pattern (blob-like or quasi-coherent mode). The measured ratio of poloidal versus radial correlation lengths is smaller than that in the conventional aspect tokamaks. The radial profile comparison of heat fluxes (Q_{conv} and Q_{cond}) and coherences of cross-fields ($\bar{\gamma}_{n\phi}$ and $\bar{\gamma}_{T\phi}$) shows that convection is main mode of the anomalous transport in ST edge. This convection may take the form of intermittent behavior, i.e. large transport events occurred in very short time

intervals. A radially sheared profile of the toroidal flow velocity Mach number has been observed, whose maximum is just located at the VSL position. This implies that the poloidal shear flow is related with the toroidal sheared plasma flow in SUNIST. Generally, the results measured in conditions of ohmically-heated discharges in SUNIST are similar to the observations in other conventional tokamaks. This similarity reflects the common qualities of the edge plasma parameters and the electrostatic fluctuations in magnetically confined devices.

Acknowledgements

The Authors are indebted to Professor C. X. Yu from Department of Modern Physics, University of Science and Technology of China for helpful discussions.

This work was sponsored by the National Natural Science Foundation of China, under Grants Nos. 10275041, 10235010 and 10375089 and supported by China Postdoctoral Science Foundation.

References

- [1] Peng Y-K M and Strickler D J *et al* 1986 *Nucl. Fusion* **26** 769
- [2] Maingi R *et al* 2003 *Plasma Phys. Control. Fusion* **45** 657
- [3] Akers R J *et al* 2002 *Phys. Rev. Lett.* **88** (21 January 2002) article #035002
- [4] Sykes A *et al* 2000 *Phys. Rev. Lett.* **84** 495
- [5] Gryaznevich M *et al* 1998 *Phys. Rev. Lett.* **80** 3972
- [6] Redd A J *et al* 2002 *Phys. Plasmas* **9** 2006
- [7] Takase Y *et al* 2001 *Nucl. Fusion* **41** 1543
- [8] Kaita R *et al* 1998 *Proc.17th IAEA Fusion Energy Conf.* paper IAEA-CN-69/CDP/12
- [9] Stambaugh R D *et al* 1996 *Proc.16th Int. Conf. Plasma Physics and Controlled Nuclear Fusion Research (Montreal, Canada)* (Vienna: IAEA)
- [10] Kotschenreuther M *et al* 2000 *Nucl. Fusion* **40** 677
- [11] Rewoldt G *et al* 1996 *Phys. Plasmas* **3** 1667
- [12] Diamond P H and Kim Y B 1991 *Phys. Fluids B* **3** 1626
- [13] Diamond P H *et al* 1994 *Phys. Rev. Lett.* **72** 2565
- [14] Zweben S J *et al* 2004 *Nucl. Fusion* **44** 134
- [15] Jain K K *et al* 2003 *Plasma Phys. Control. Fusion* **45** 1283
- [16] Synakowski E J *et al* 2002 *Plasma Phys. Control. Fusion* **44** A165
- [17] Wang Y *et al* 2003 *Plasma Science & Technology* **5** 2017
- [18] Chen Sin-Li and Sekiguchi T 1965 *J. Appl. Phys.* **36** 2363
- [19] Powers E J 1974 *Nucl. Fusion* **14** 749
- [20] Ross D W 1992 *Plasma Phys. and Control. Fusion* **34** 137.
- [21] Beall J M, Kim Y C and Powers E J 1982 *J. Appl. Phys.* **53** 3933
- [22] Stangeby P C and McCracken G M 1990 *Nucl. Fusion* **30** 1225
- [23] Chung K-S and Hutchinson I H 1988 *Phys. Rev A* **38** 4721
- [24] Ritz Ch P *et al* 1984 *Phys. Fluids* **27** 2956
- [25] Burrell K H 1999 *Phys. Plasmas* **6** 4418
- [26] Carcía-Cortés I *et al* 2000 *Plasma Phys. Control. Fusion* **42** 389

- [27] Bengston R D , Back R and Chung K-S 1995 *Bull. Am. Phys. Soc.* 40 1810
- [28] Dong J Q, Horton W, Bengston R D and Li G X 1994 *Phys. Plasmas* **1** 3250
- [29] Mattor N, Diamond P H 1994 *Phys. Rev. Lett.* **72** 486
- [30] Mattor N, Diamond P H 1994 *Phys. Plasmas* **1** 4002
- [31] Mattor N 1995 *Phys. Plasmas* **2** 766
- [32] Xu Y H *et al* 1996 *Phys. Plasmas* **3** 1022
- [33] Wootton A J *et al* 1990 *Phys. Fluids B* **2** 2879
- [34] Ritz Ch P *et al* 1987 *Nucl. Fusion* **27** 1125
- [35] Huber A *et al* 1999 *J. Nucl. Mater.* **266-269** 546
- [36] Wang G *et al* 2000 *Plasma Phys. Control. Fusion* **42** 127
- [37] Bleuel J *et al* 2002 *New J. Phys.* **4** 38.1
- [38] Singh A K, Morelli J, Asai T and Hirose A 2003 *Phys. Plasmas* **10** 3451
- [39] Singh A K, Kaur R, Mattoo S K and Hirose A 2004 *Phys. Plasmas* **11** 328
- [40] Rudakov D L *et al* 2002 *Plasma Phys. Control. Fusion* **44** 717
- [41] Boedo J A *et al* 2001 *Phys. Plasmas* **8** 4826
- [42] Carreras B A *et al* 2000 *Phys. Plasmas* **7** 3278
- [43] Jha R *et al* 1992 *Phys. Rev. Lett.* **69** 1375
- [44] Sanchez E *et al* 2000 *Phys. Plasmas* **7** 1408
- [45] Carbone V *et al* 2000 *Phys. Plasmas* **7** 445
- [46] Fillippas A V *et al* 1995 *Phys. Plasmas* **2** 839
- [47] Boedo J A *et al* 2001 *Phys. Plasmas* **8** 4826
- [48] Carreras B A *et al* 1996 *Phys. Plasmas* **3** 2664
- [49] Davis A, Marshak A, Wiscombe W and Cahalan R 1996 *J. Atmos. Sci.* **53** 1538
- [50] Carreras B A, Lynch V E and LaBombard B 2001 *Phys. Plasmas* **8** 3702

List of Figure Captions

Figure 1. Schematic view of the SUNIST vacuum vessel and coils layout. All of three probe arrays are set on the outer midplane of the device.

Figure 2. Relative position of two windows where the probe arrays are laid, and a closed-up view of the probe structures. Tip 1 ~ tip 4 constitutes the triple probe, tip 5 ~ tip 7 are used to measure floating potentials, and tip 8 ~ tip 9 forms the Mach probe.

Figure 3. Typical discharge waveforms of (a) the plasma current, (b) loop voltage, (c) ion saturation current and (d) floating potential.

Figure 4. Radial profiles of equilibrium T_e , n_e , ϕ_f and ϕ_p . In (b) the dotted curve is the seventh-polynomial fit of the ϕ_p . The error bars are the statistical errors of the ensemble average. The shadow region stands for the radial location of the limiter.

Figure 5. Radial profiles of radial electric field E_r and its radial gradient dE_r/dr .

Figure 6. Radial profiles of toroidal flow velocity Mach number M . The error bars are the statistical errors of the ensemble average.

Figure 7. Radial profiles of (a) the absolute RMS fluctuations \tilde{n}_e , \tilde{T}_e and $\tilde{\phi}_p$; and (b) relative fluctuation levels \tilde{n}_e/n_e , \tilde{T}_e/T_e and $e\tilde{\phi}_p/kT_e$.

Figure 8. (a) Contour plot of the estimated conditional wavenumber-frequency spectrum $s(k_r | f)$, (b) radial wavenumber spectrum $S(k_r)$, (c) the spectral-averaged statistical dispersion relation $k_r(f)$ and the wavenumber spectral width $\sigma_{k_r}(f)$ at $r = 50$ cm. (d) Radial profiles of the radial spectral-averaged wavenumber \bar{k}_r and radial phase velocity v_{phr} . Positive k_r represents the radially outward direction.

Figure 9. Radial profiles of (a) the poloidal spectral-averaged wavenumber \bar{k}_θ and (b) poloidal and radial correlation lengths, $l_{c\theta}$ and l_{cr} , respectively.

Figure 10. Radial profiles of (a) the radial particle fluxes Γ_r , (b) the radial heat fluxes Q_r , Q_{conv} and Q_{cond} ; (c) the coherence $\bar{\gamma}_{n\phi}$ and $\bar{\gamma}_{T\phi}$; and (d) the spectral-averaged phase angle $\bar{\alpha}_{n\phi}$ and $\bar{\alpha}_{T\phi}$.

Figure 11. Typical time evolutions of $\Gamma_r(t)$ at plasma edge (a) and at SOL (b); (c) and (d) are the corresponding conditional averaging results for the signals in (a) and (b), respectively.

Figure 12. (a) *PDFs* and (b) auto-power spectra of Γ_r , data are the same as in figure 11(a) and 11 (b).

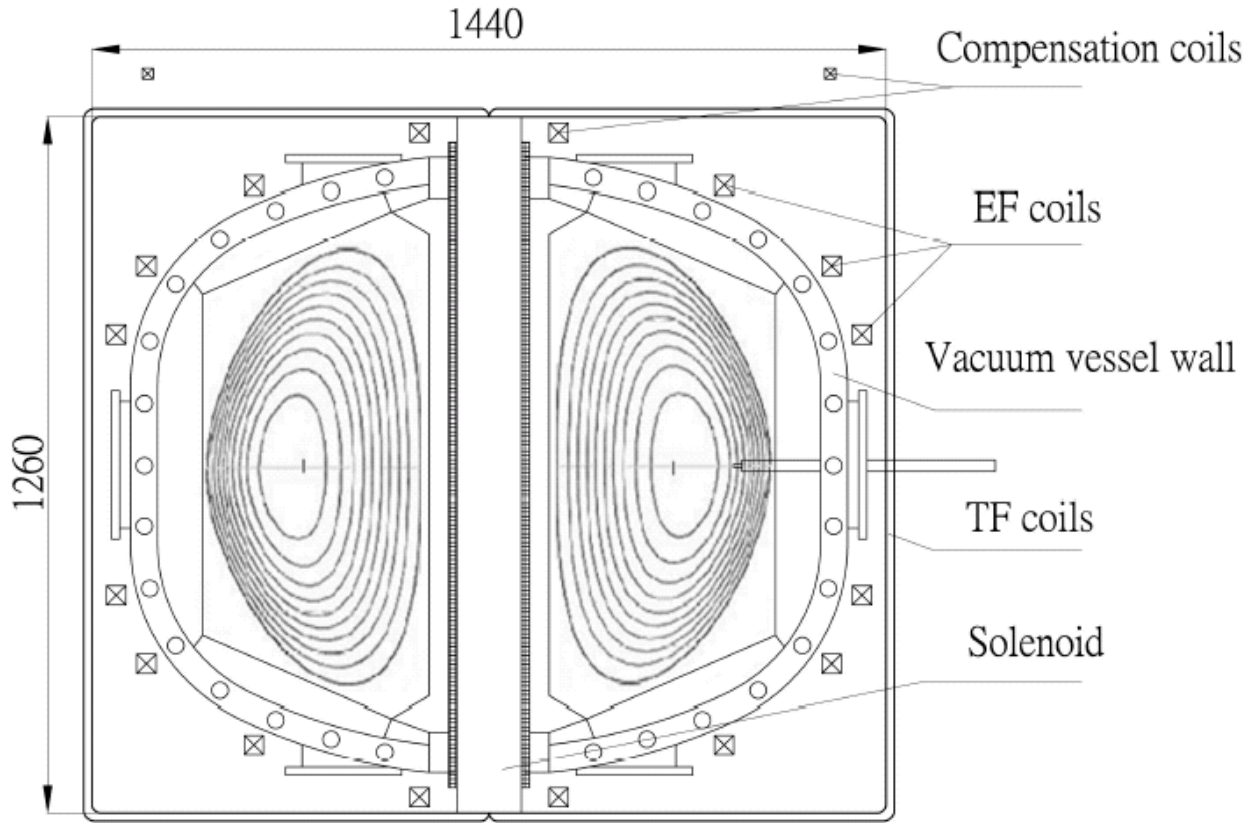


Fig 1

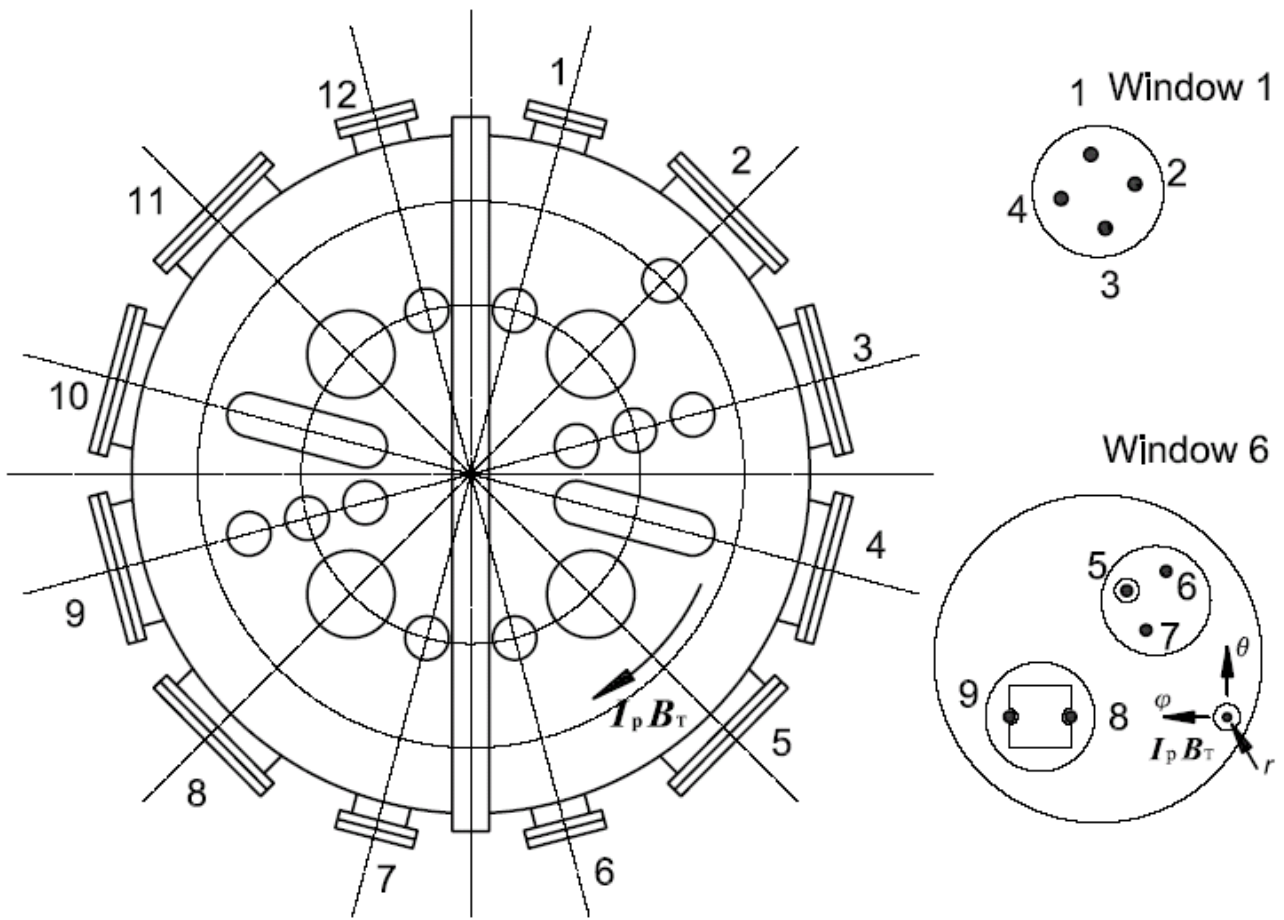


Fig. 2

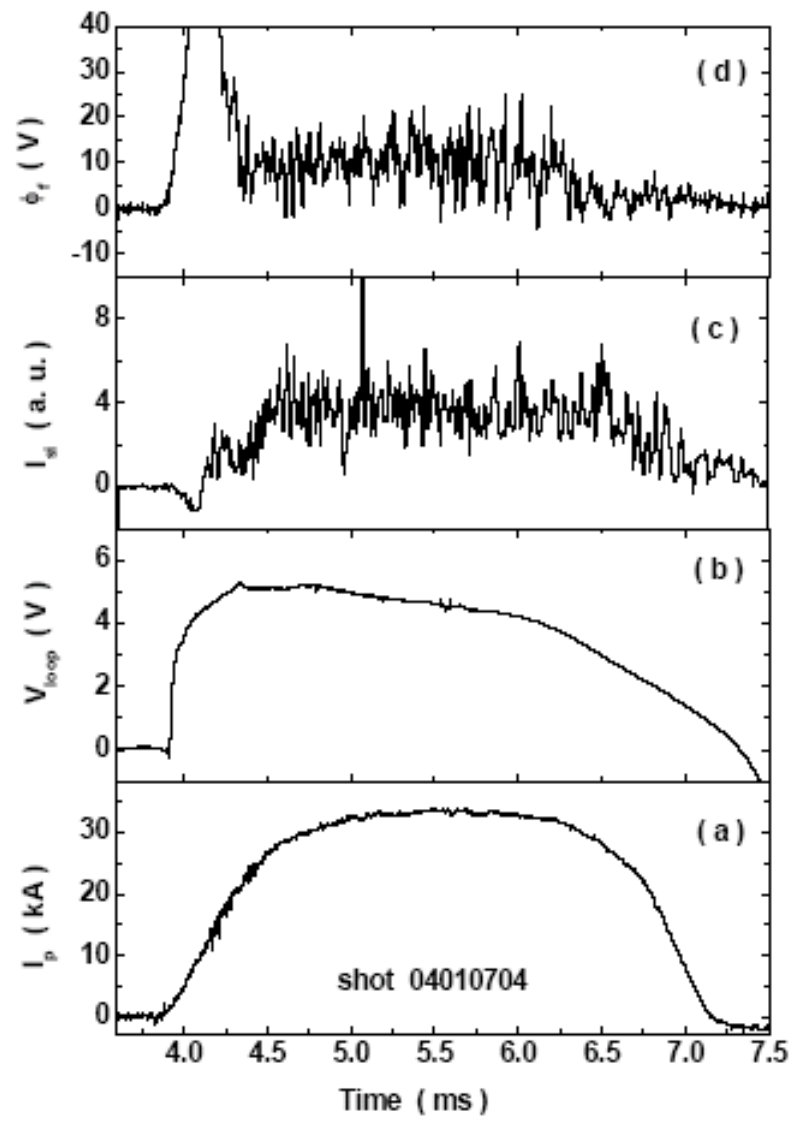


Fig. 3

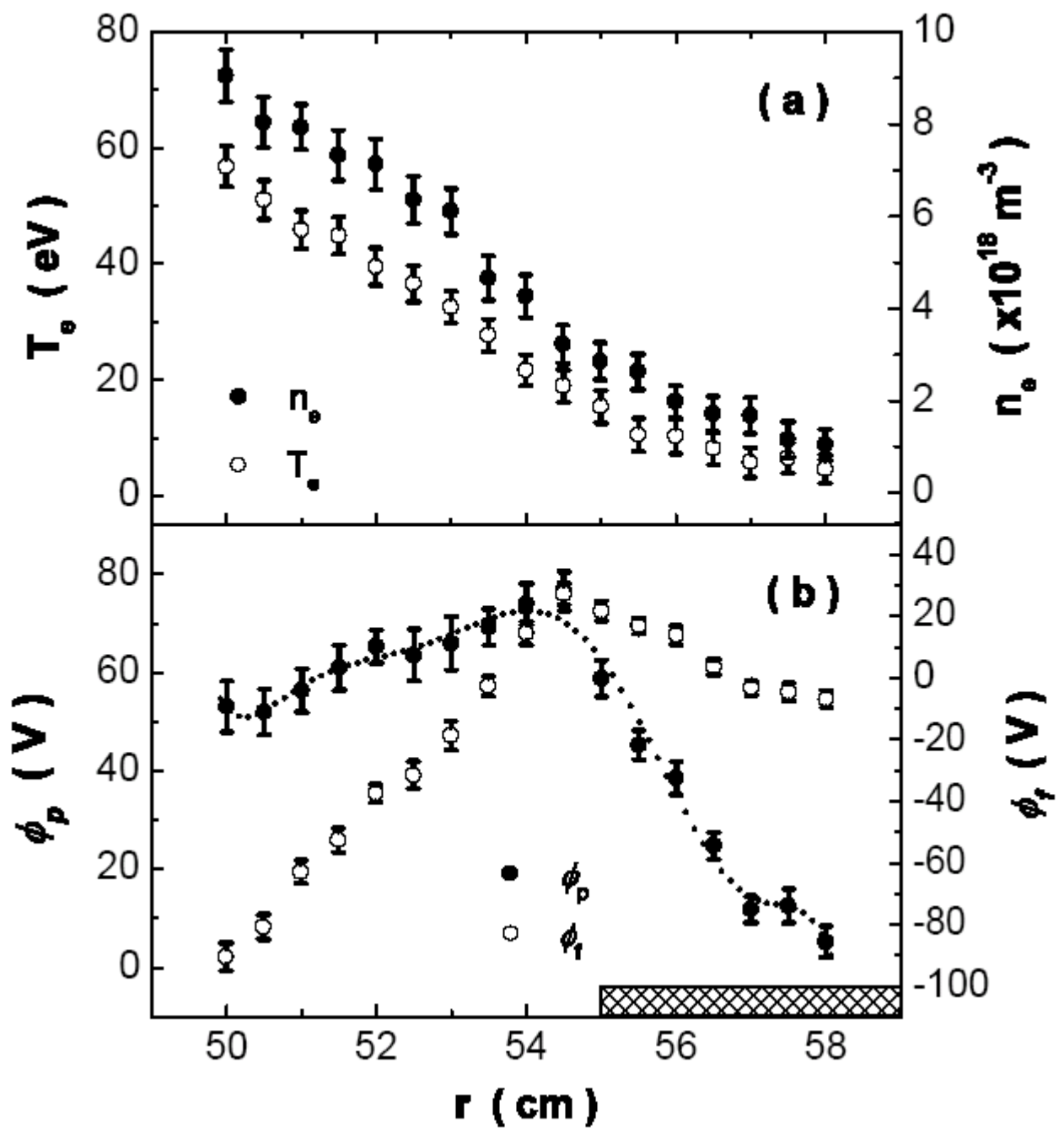


Fig. 4

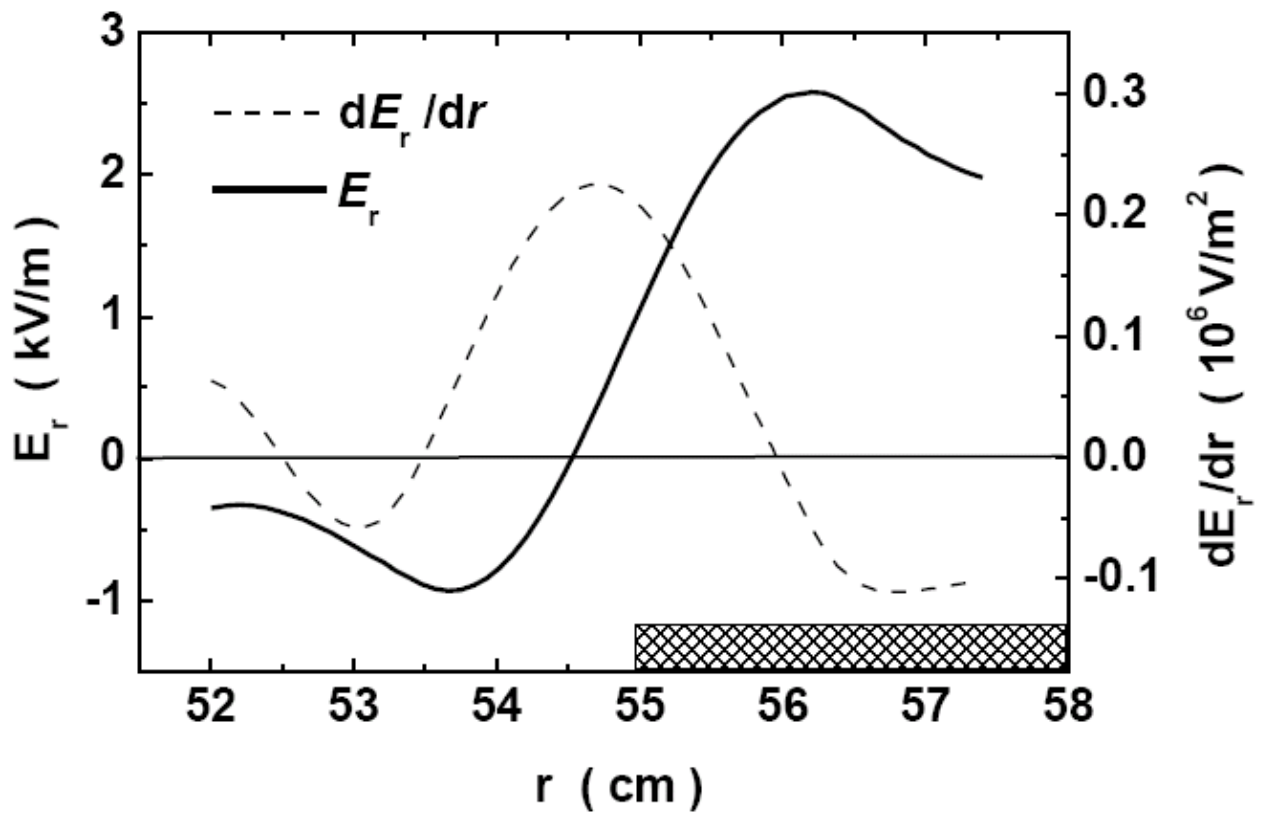


Fig. 5

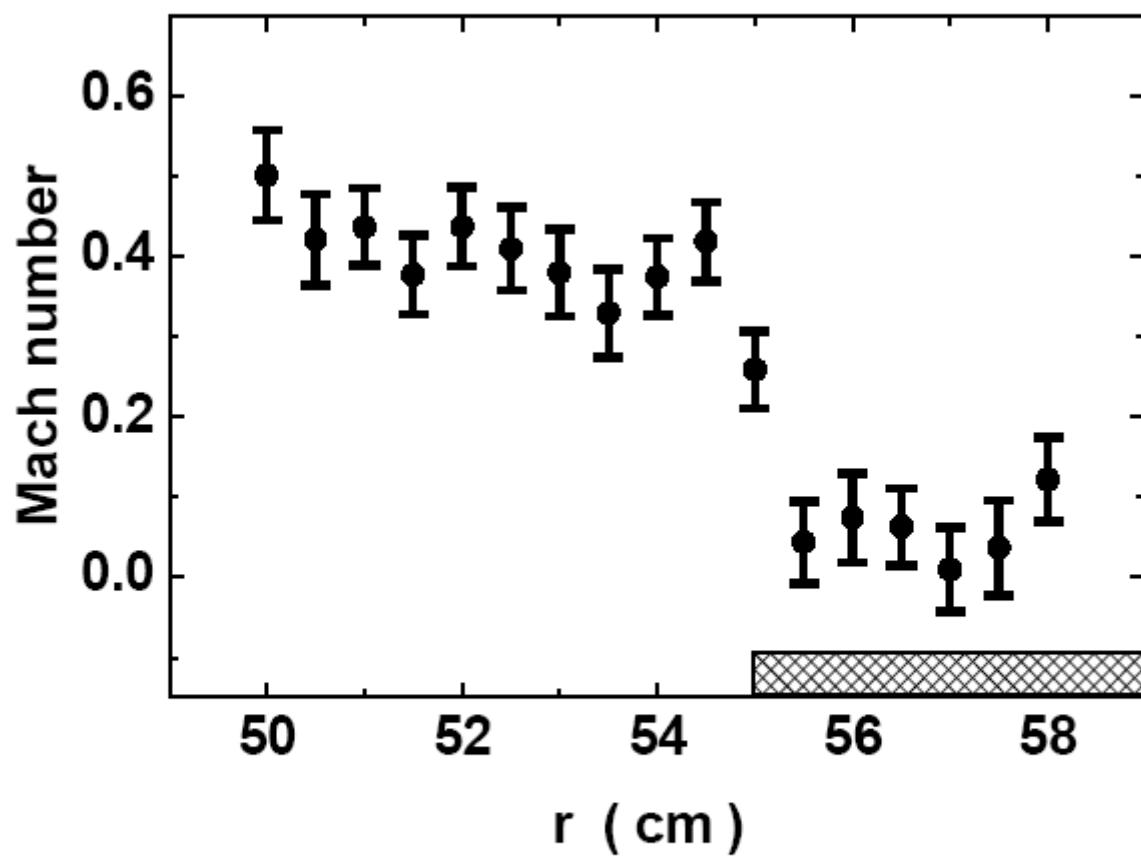


Fig. 6

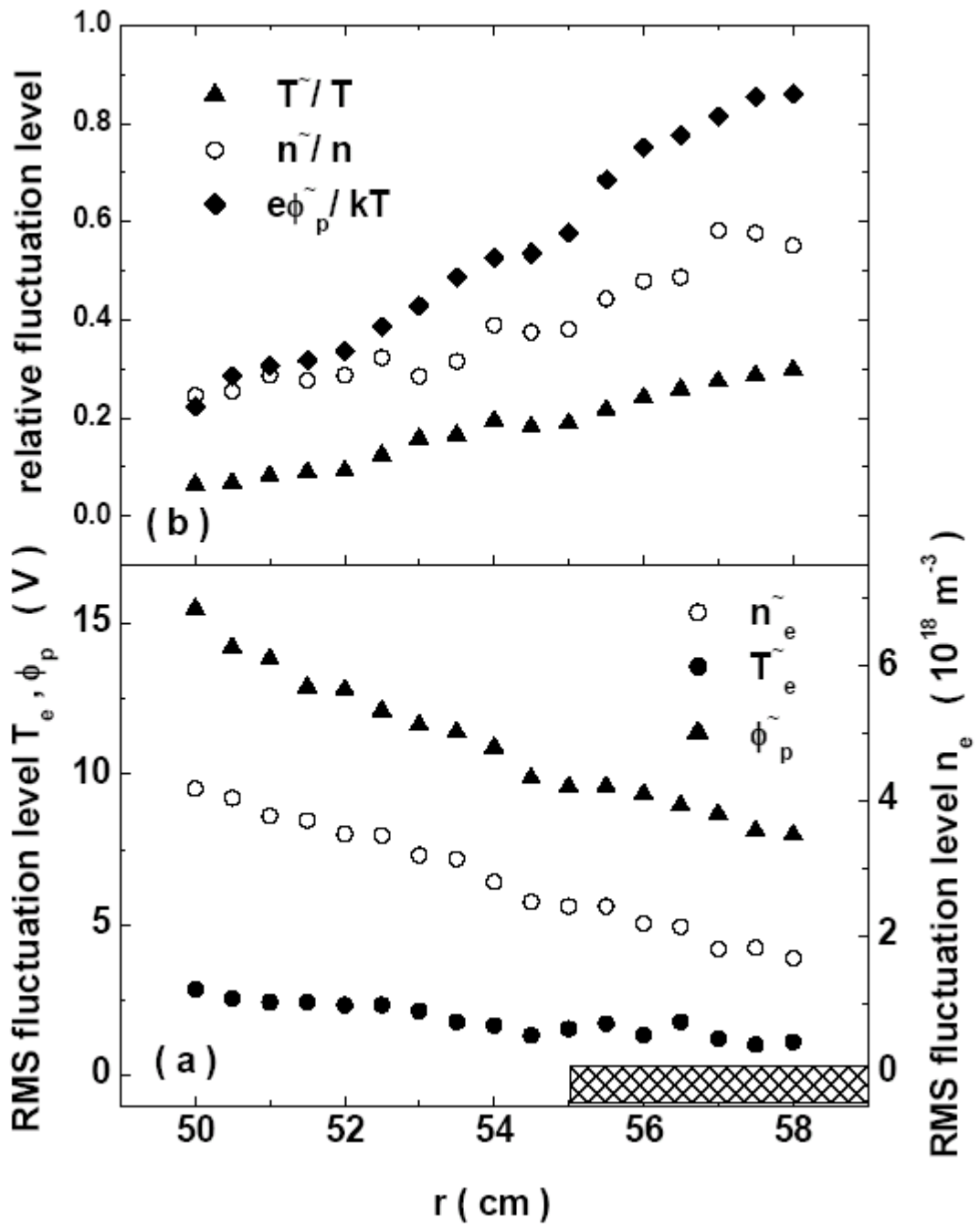


Fig.7

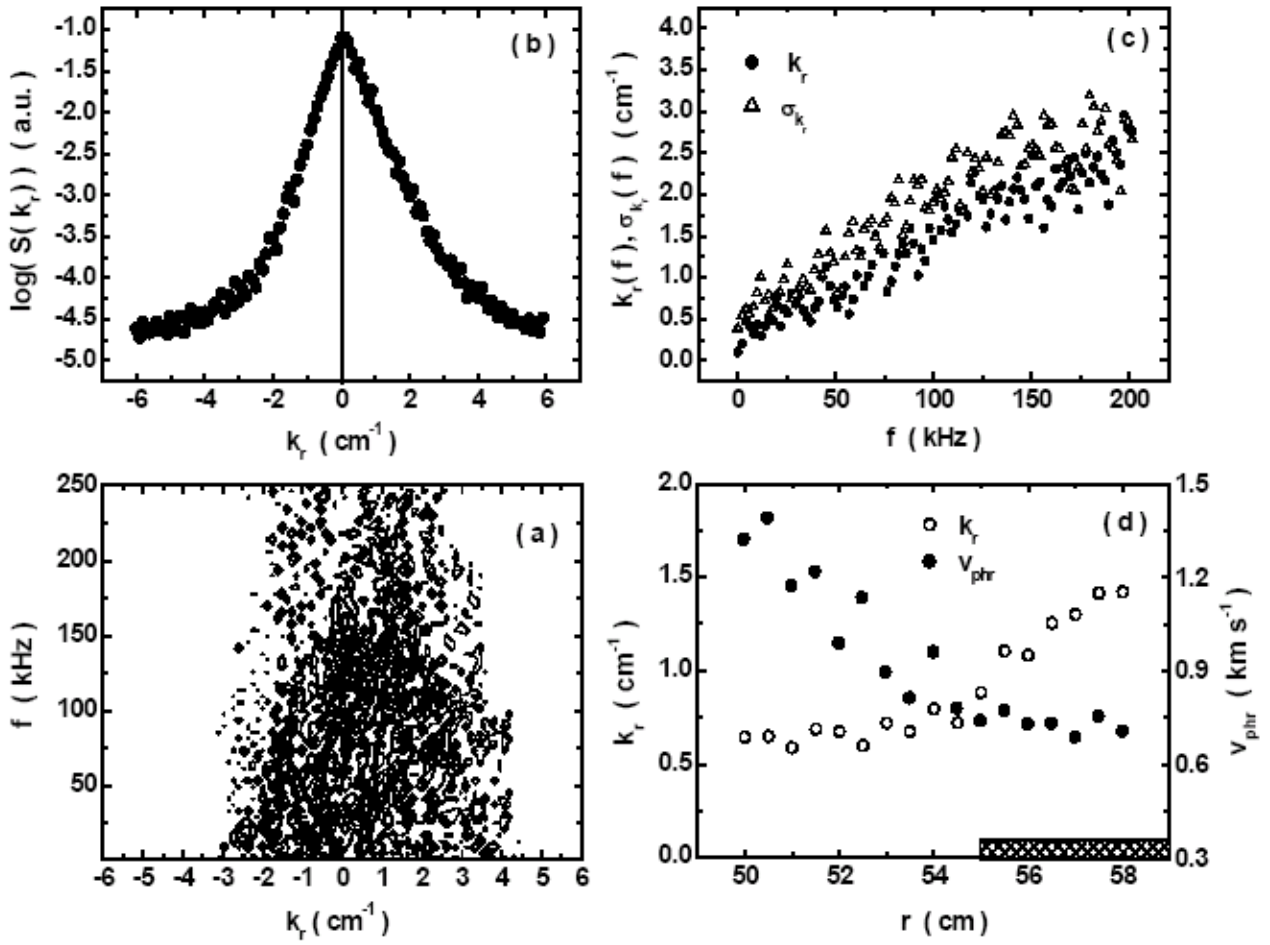


Fig. 8

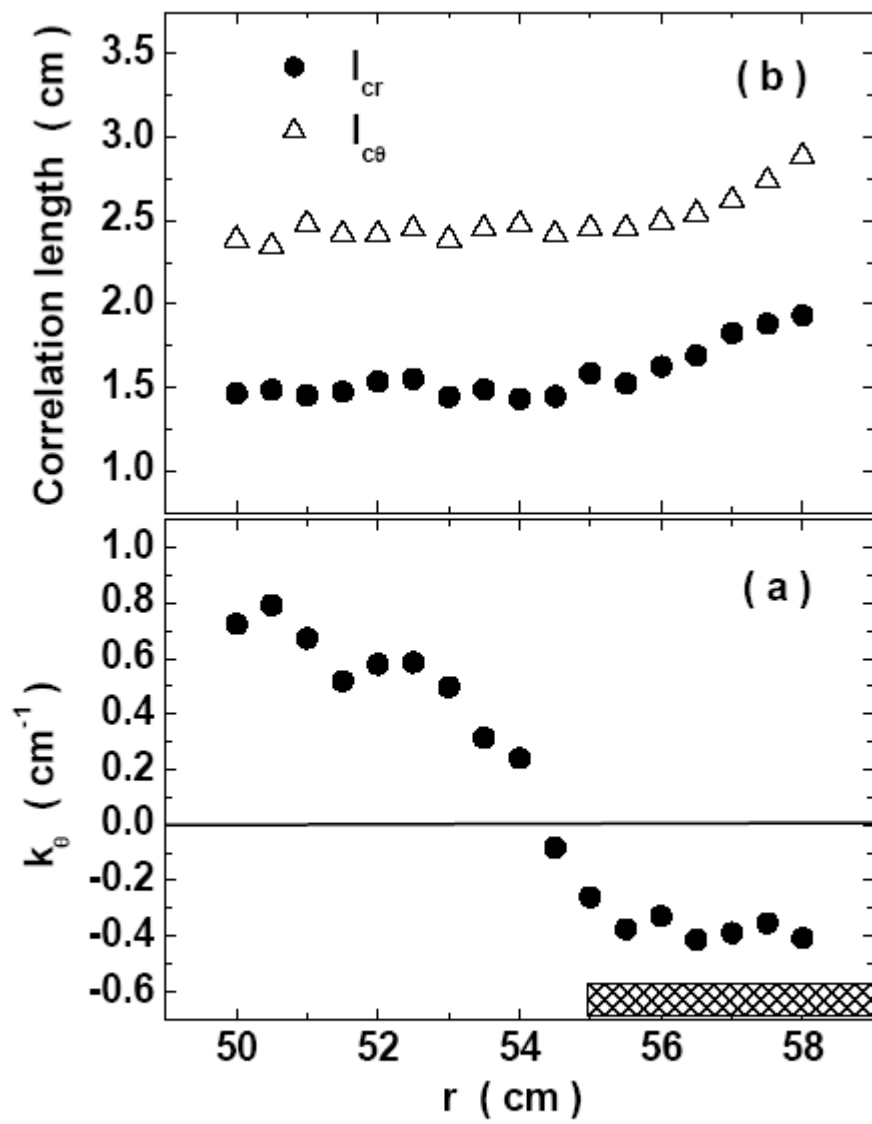


Fig. 9

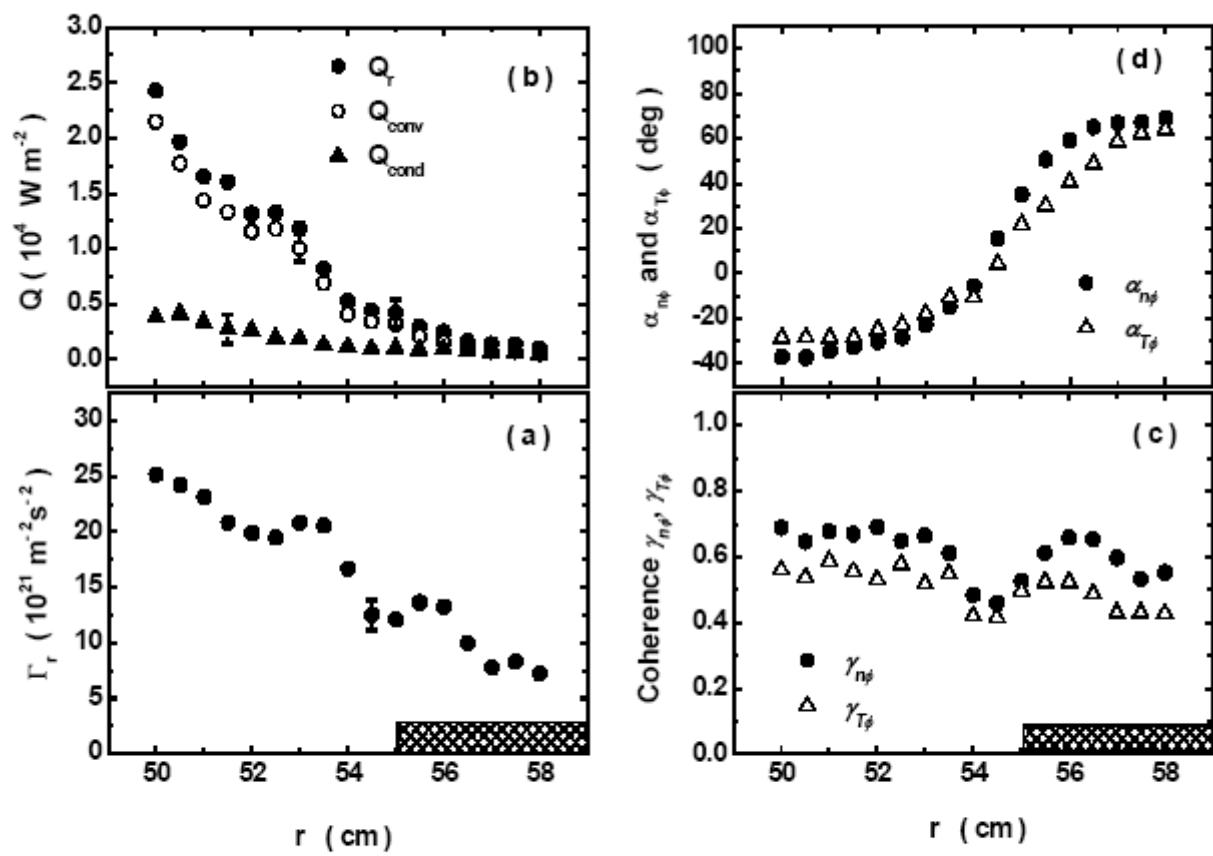


Fig. 10

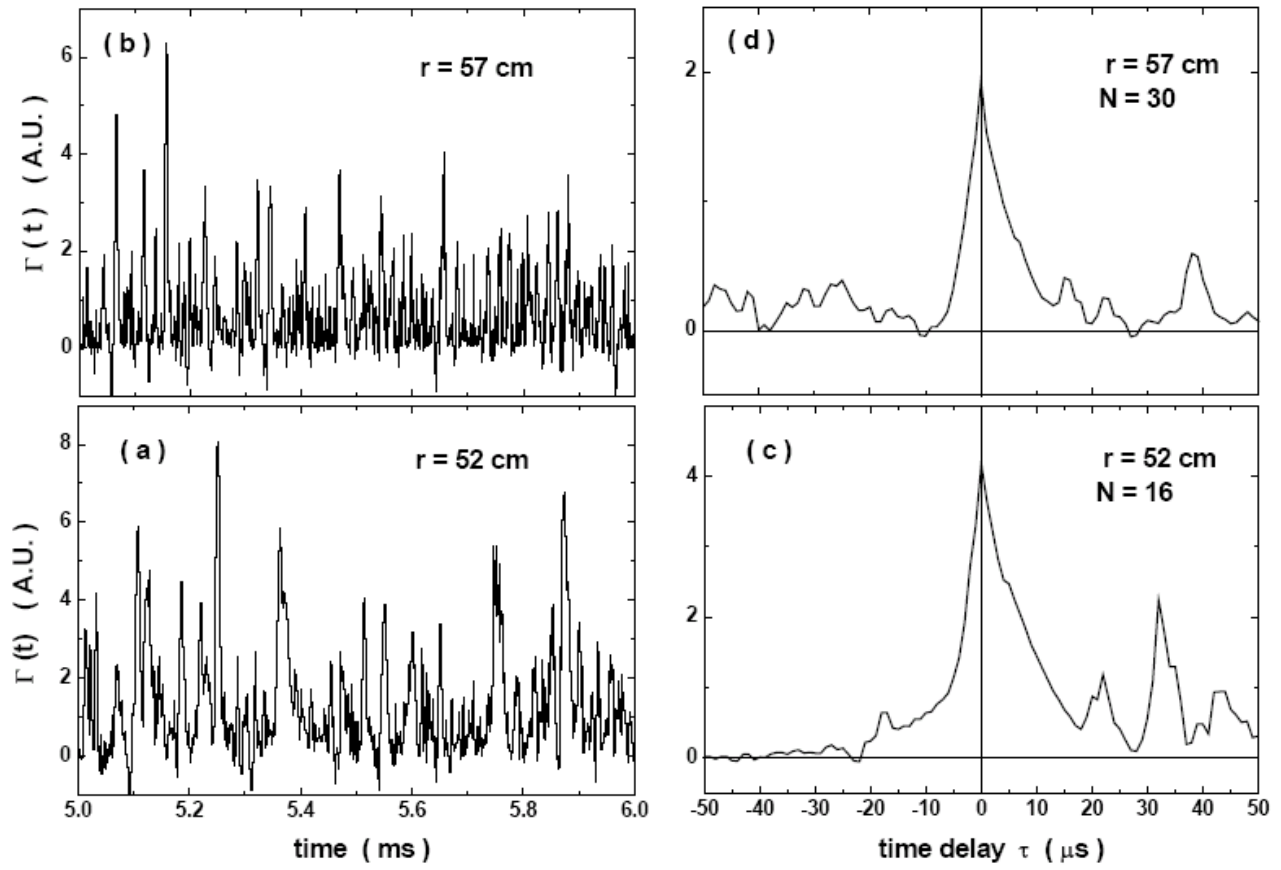


Fig. 11

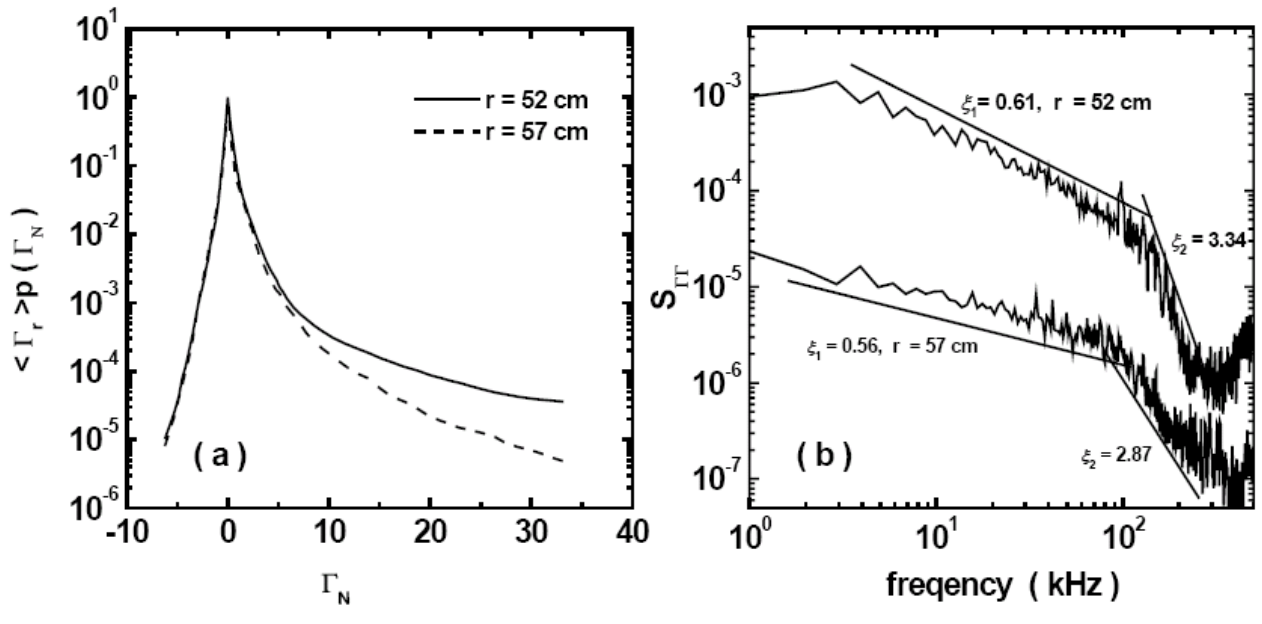


Fig. 12